

Dark Energy in Ghost-free non-local Gravity

S.D. Odintsov,^{1,2,*} V.K. Oikonomou,^{3,4,†} and G.S. Sharov^{5,6,‡}

¹*ICREA, Passeig Luis Companys, 23, 08010 Barcelona, Spain*

²*Institute of Space Sciences (IEEC-CSIC) C. Can Magrans s/n, 08193 Barcelona, Spain*

³*Physics Department, Observatory, Aristotle University of Thessaloniki, Thessaloniki, Greece*

⁴*Center for Theoretical Physics, Khazar University,*

41 Mehseti Str., Baku, AZ-1096, Azerbaijan

⁵*Tver state university, Sadovyy per. 35, 170002 Tver, Russia*

⁶*International Laboratory for Theoretical Cosmology,*

Tomsk State University of Control Systems and Radioelectronics (TUSUR), 634050 Tomsk, Russia

Ghost-free non-local gravity is investigated with regards to its late-time dynamics. Viable solutions in this model are confronted with the observational data including the Pantheon+ catalogue of Type Ia supernovae, the Dark Energy Spectroscopic Instrument, the measurements of baryon acoustic oscillations and the Hubble parameter estimations $H(z)$. The ghost-free non-local gravity is found to be successful in these tests in comparison to the Λ CDM model and can be also comparable with the generalized exponential $F(R)$ gravity scenario. However the model encounters difficulties when the data from the above observations and the cosmic microwave background radiation data are combined. In tests with the whole set of Pantheon+, DESI, $H(z)$ and CMB data, the generalized exponential $F(R)$ model is essentially more successful. This success is related with the dynamical behavior of its effective dark energy equation of state evolving from a phantom to a quintessence phase during the late-time epoch, whereas the ghost-free non-local model demonstrates only a quintessence behavior. Hence the ghost-free non-local gravity scenario is successful only when the Pantheon+, DESI and $H(z)$ data are considered. The generalized exponential $F(R)$ model satisfies the viability conditions and in tests with all observational data including CMB surpasses the Λ CDM model in χ^2 statistics and also with information criteria.

I. INTRODUCTION

During the last two years, one can see groundbreaking changes in observational cosmology based on the new observations of Baryon Acoustic Oscillations (BAO) from the Dark Energy Spectroscopic Instrument (DESI) [1, 2] along with the Type Ia Supernovae (SNe Ia) data from the Pantheon+, Union3, DES5Y catalogues [3–5]. These new observational data can shed light on the nature and properties of dark energy that drives the late-time accelerated expansion of the Universe observed during last three decades. This acceleration and dark energy as its origin, is successfully described in the frameworks of the Λ -Cold-Dark-Matter model (Λ CDM) with the cosmological constant Λ playing the role of dark energy, with the equation of state (EoS) for dark energy is constant: $P_{DE}/\rho_{DE} = -1$ [6].

The Λ CDM model during last decades encountered several problems in theory and observations, including vague physical nature of its dark components, the coincidence problem of their densities nowadays, the fine-tuning for Λ , the Hubble constant tension and other questions about dark matter and dark energy induced numerous alternative cosmological scenarios including modifications of General Relativity (see reviews [6–9]). Cosmologists suggested different approaches for solving the problems related with the dark energy nature and structure and several scenarios explaining the Hubble constant tension between early-time estimations of H_0 from Cosmic Microwave Background radiation (CMB) [10], and local distance-ladder measurements by SH0ES collaboration were proposed [11–25].

The strongest challenge for the Λ CDM model appeared two years ago and was further confirmed in 2025 with new BAO DESI data [1, 2]. These data contradicted constant EoS for dark energy corresponding to the Λ CDM model in favor of a dynamical or variable dark energy EoS $w_{DE} = P_{DE}/\rho_{DE} = w_{DE}(z)$ which evolves from a phantom to a quintessence EoS during the late-time epoch [26–38].

Effective dynamical dark energy may be generated not only in models with a given variable EoS, but also in modified gravity theories, in particular, in $F(R)$ gravity theories with non-trivial dependence on the Ricci scalar R in the Lagrangian [35–59]. These models are in general motivated by UV-completions of Einstein gravity, and can unify the late-time epoch with the early-time inflationary era.

Another approach in modelling modified gravity, which is also motivated from the quantum effective theory, is non-local theory of gravity [60–72]. In particular, it was shown in Ref. [71] that a non-local $F(R)$ gravity can be transformed into a ghost-free local $F(R, \phi)$ model by introducing a scalar field ϕ . In paper [72] the inflationary stage of this model was investigated and predicted inflationary parameters appeared to be compatible with the latest Atacama Cosmology Telescope and Planck constraints [73–75].

* odintsov@ieec.cat

† v.k.oikonomou1979@gmail.com;voikonomou@gapps.auth.gr

‡ sharov.gs@tversu.ru

In this paper, we test the late-time dynamics of the $F(R, \phi)$ model [71, 72] originated from the non-local $F(R)$ gravity. We confront this model with Pantheon+ SNe Ia [3], BAO DESI RD2 [2], the Hubble parameter observational data and compare this model with the Λ CDM and the generalized exponential $F(R)$ scenarios.

This article is organized as follows: in section II, the dynamical equations for $F(R, \phi)$ gravity during its late-time evolution are described. In section III the generalized exponential $F(R)$ model is investigated. In the next section the results of observational tests with SNe Ia, $H(z)$ and BAO DESI data are described for both the considered models in comparison with the Λ CDM scenario. In section V the models are confronted with the mentioned observations along with CMB data. In the final section, the main results and conclusions are presented.

II. DYNAMICS OF GHOST-FREE NON-LOCAL GRAVITY AND ITS FORMULATION IN TERMS OF $F(R, \phi)$ GRAVITY

In the article [71], the non-local gravity model with the action,

$$S = \int d^4x \sqrt{-g} \left\{ \frac{1}{2\kappa^2} \left(R - \frac{1}{2} F(R) \square^{-1} F(R) \right) + \mathcal{L}_{\text{matter}} \right\}. \quad (2.1)$$

has been proposed. The model is based on $F(R)$ gravity, where R is the Ricci scalar, $\mathcal{L}_{\text{matter}}$ is the matter Lagrangian density. This scenario has no ghost degrees of freedom.

The gravitational action (2.1) with the non-local operator \square^{-1} in Ref. [72] was transformed by using a scalar field ϕ to the following form,

$$S = \int d^4x \sqrt{-g} \left\{ \frac{R}{2\kappa^2} - \frac{1}{2} \partial_\mu \phi \partial^\mu \phi - \phi F(R) f(R, \phi) + \mathcal{L}_{\text{matter}} \right\}. \quad (2.2)$$

Following Ref. [72], we use the notation,

$$f(R, \phi) = \frac{R}{\kappa^2} - \partial_\mu \phi \partial^\mu \phi - 2\phi F(R) \quad (2.3)$$

with its derivatives f_R and f_ϕ :

$$f_R = \frac{\partial f(R, \phi)}{\partial R} = \frac{1}{\kappa^2} - 2\phi F'(R), \quad f_\phi = \frac{\partial f}{\partial \phi} = -2F(R).$$

In the flat Friedmann-Lemaître-Robertson-Walker (FLRW) background metric,

$$ds^2 = -dt^2 + a(t)^2 \sum_{i=1,2,3} (dx^i)^2, \quad (2.4)$$

the dynamical equations resulting from variations of the action (2.2) with respect to the metric and the scalar field ϕ , take the form [76],

$$3H^2 f_R = \rho + \dot{\phi}^2 + \frac{R f_R - f}{2} - 3H \dot{f}_R, \quad (2.5)$$

$$-(3H^2 + 2\dot{H}) f_R = P - \frac{R f_R - f}{2} + \ddot{f}_R + 2H \dot{f}_R, \quad (2.6)$$

$$0 = \ddot{\phi} + 3H \dot{\phi} + F(R). \quad (2.7)$$

Here, the ‘‘dot’’ denotes the derivative with respect to the cosmic time t , ρ and P are energy density and pressure for dark matter and dark matter and radiation.

In the Ref. [72], the inflationary cosmology of the model (2.2) was considered for the power-law $F(R)$ function

$$F(R) = -\alpha R^n \quad (2.8)$$

for two cases, where the constant n lies in the interval $1 < n < 2$, and for $n = 2$. Under the slow-roll conditions for the Hubble rate $\dot{H} \ll H^2$ and for the scalar field $\ddot{\phi} \ll H\dot{\phi}$ in Ref. [72] the slow-roll indices and the inflationary parameters have been calculated and was shown that the spectral index of scalar perturbation n_s and the tensor-to-scalar ratio r predicted in the model (2.2), (2.8) satisfy the latest Planck/BICEP and Atacama Cosmology Telescope (ACT) constraints [73–75].

In this article, we study the late-time evolution of the considered $F(R, \phi)$ model that can be confronted with available observational data. Unlike the inflationary epoch, at late times the matter terms ρ and P

in Eqs. (2.5), (2.6) are essential in the late-time dynamics of the Universe. These equations lead to their standard FLRW evolution,

$$\rho = \rho_m^0 a^{-3} + \rho_r^0 a^{-4} = \rho_m^0 (a^{-3} + X_r a^{-4}), \quad (2.9)$$

where we fix the present day radiation to matter ratio [36, 37]

$$X_r = \rho_r^0 / \rho_m^0 = 2.9656 \cdot 10^{-4}.$$

Equation (2.9), the relation,

$$R = 12H^2 + 6\dot{H} \quad (2.10)$$

together with the Eq. (2.5) in the form [72]

$$\frac{3}{\kappa^2} H^2 = \rho + \frac{\dot{\phi}^2}{2} + \phi [F(R) - RF'(R)] + 6H [(H\phi + \dot{\phi})F'(R) + \phi F''(R)\dot{R}] \quad (2.11)$$

and Eq. (2.7) form the system of dynamical equations for the considered $F(R, \phi)$ model.

In these equations with the power-law $F(R)$ function (2.8) we use the dimensionless (normalized) variables $E, \mathcal{R}, \Phi, \Psi$

$$E = \frac{H}{H_0}, \quad \mathcal{R} = \frac{R}{2\Lambda}, \quad \Phi = \kappa\phi, \quad \Psi = \frac{\kappa\dot{\phi}}{H_0} \quad (2.12)$$

instead of the Hubble parameter H , the Ricci scalar R , the functions ϕ and $\dot{\phi}$. We also use the dimensionless free model parameters

$$\Omega_m^0 = \frac{\kappa^2 \rho_m^0}{3H_0^2}, \quad A = 2\kappa(2\Lambda)^{n-1}\alpha, \quad (2.13)$$

representing the cold matter nowadays fraction and the constant α in Eq. (2.8) respectively. Here $H_0 = H(t_0)$ is the Hubble constant, the constant Λ is associated with the cosmological constant, though dark energy in this model is generated by the $F(R)$ term and the scalar ϕ , hence Λ is not considered as a free parameter, but it is expressed via Ω_m^0 and H_0 as follows:

$$\Omega_\Lambda = \frac{\Lambda}{3H_0^2} = 1 - \Omega_m^0(1 + X_r).$$

In the notation of Eqs. (2.12) and (2.13) with the parameter $x = \log a$ instead of t (where $\frac{d}{dt} = H \frac{d}{dx}$) the dynamical equations (2.10), (2.11) and (2.7) can be rewritten in the following form,

$$\frac{dE}{dx} = \Omega_\Lambda \frac{\mathcal{R}}{E} - 2E, \quad (2.14)$$

$$\frac{d\mathcal{R}}{dx} = \frac{\Omega_m^0 (a^{-3} + X_r a^{-4}) - E^2 + \frac{1}{6}\Psi^2 + A\mathcal{R}^n [(n-1)\Omega_\Lambda\Phi - nE(E\Phi + \Psi)/E]}{n(n-1)A\Phi E^2 \mathcal{R}^{n-2}}, \quad (2.15)$$

$$\frac{d\Phi}{dx} = \frac{1}{E}\Psi, \quad (2.16)$$

$$\frac{d\Psi}{dx} = -3\Psi + 3A\Omega_\Lambda \frac{\mathcal{R}^n}{E}. \quad (2.17)$$

This system of equations can be integrated numerically over the variable $x = \log a$ “into the past”, if we start from the initial conditions at the present time $t = t_0$ or $x = 0$,

$$E|_{x=0} = 1, \quad \mathcal{R}|_{x=0} = \mathcal{R}_0, \quad \Phi|_{x=0} = \Phi_0, \quad \Psi|_{x=0} = \Psi_0. \quad (2.18)$$

These numerical solutions are determined if we fix seven free model parameters including five constants (2.13), (2.18), n and the Hubble constant,

$$\Omega_m^0, \quad n, \quad A, \quad \mathcal{R}_0, \quad \Phi_0, \quad \Psi_0, \quad H_0. \quad (2.19)$$

For any solution $E = E(a)$ and the fixed value H_0 we obtain the Hubble parameter $H(a) = H_0 E$ as a function of the scale factor or $H = H(z)$ as a function of redshift

$$z = \frac{1}{a} - 1$$

that can be compared with observational data.

For the considered $F(R, \phi)$ model, (2.2), (2.8) integral curves of the system (2.14)–(2.17) do not diverge into the “past” direction, this behavior differs from $F(R)$ models explored in the papers [36–38] and the generalized exponential $F(R)$ model (see Sect. III), where we could integrate similar systems only “into the future”. This feature is the essential advantage of the $F(R, \phi)$ model. However, viable cosmological solutions of the system (2.14)–(2.17) exist not for all values of model parameters (2.19). For example, to exclude singularities in the past we should choose only negative values of Φ_0 (with large $|\Phi_0|$) in the initial conditions (2.18) and fix other model parameters under some restrictions. These restrictions become more narrow if we confront model predictions with observational data, including the Pantheon+ catalogue of Type Ia supernovae (SNe Ia) [3], the DESI measurements of baryon acoustic oscillations [2] and the Hubble parameter estimations $H(z)$. The calculated solutions $H(z)$ are tested with these

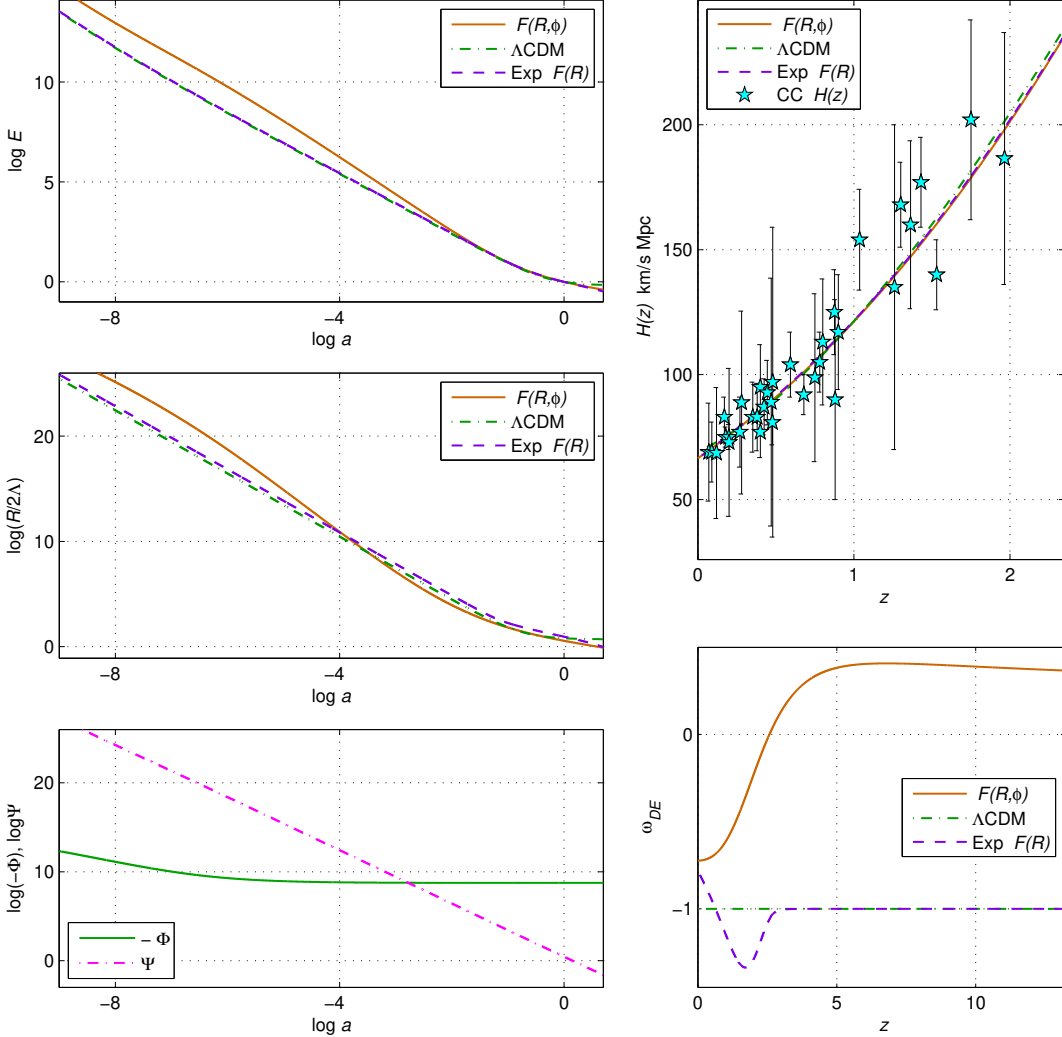


FIG. 1. Evolution of the normalized Hubble parameter E , Ricci scalar \mathcal{R} and the scalar field $-\Phi$, Ψ in logarithmic scale for the $F(R, \phi)$ model (2.2), (2.8) (the left panels), the Hubble parameter $H(z)$ and the dark energy EoS parameter $\omega_{DE}(z)$ as functions of redshift (the right panels) in comparison to the Λ CDM model (2.20) and the generalized exponential $F(R)$ model (3.1). The model parameters for 3 models are fixed from Table IV.

observations and we obtain the best fit values of the free model parameters (2.19) for the $F(R, \phi)$ model. These best fits are tabulated in Table IV below where we compare the results with two other models.

The behavior of these solutions is shown in Fig. 1 where the evolution of the normalized Hubble parameter $E = H/H_0$, Ricci scalar $\mathcal{R} = \frac{R}{2\Lambda}$ and the scalar field parameters Φ , Ψ is presented in comparison with similar variables in the Λ CDM model,

$$H^2 = H_0^2 [\Omega_m^0 (a^{-3} + X_r a^{-4}) + \Omega_\Lambda] \quad (2.20)$$

and the generalized exponential $F(R)$ model described below in section III. For all the models, the best fit parameters from Table IV are used in Fig. 1. In the left panels we draw logarithms: $\log E$, $\log \mathcal{R}$,

$\log(-\Phi)$ and $\log \Psi$ as functions of $x = \log a$. One can see that for the $F(R, \phi)$ model the Ricci scalar \mathcal{R} at $z > 100$ ($a < 10^{-2}$) exceeds this value for the Λ CDM model. The similar behavior takes place for $E(a)$, but for the best fit solution in the $F(R, \phi)$ model this difference is reduced to minimal values.

In the top-right panel of Fig. 1 the Hubble parameter $H(z)$ depending on redshift z is depicted for three models and is compared with $H(z)$ observational data. And in the bottom-right panel the dark energy EoS parameter,

$$\omega_{DE}(z) = \frac{P_{DE}}{\rho_{DE}} = -1 + \frac{1}{3} \frac{d}{dx} \log [E^2 - \Omega_m^0 (a^{-3} + X_r a^{-4})]. \quad (2.21)$$

is shown for the same best fitted $E(z)$. Here ρ_{DE} is the effective DE density generated by ϕ and $F(R)$ gravity, ρ_{DE} is the additional summand to ρ in the right hand side of Eq. (2.11). The effective DE pressure P_{DE} can similarly be extracted from Eq. (2.6). For the Λ CDM model the dark energy EoS parameter is constant $\omega_{DE} = -1$, but for the model (2.2), (2.8) it behaves as variable quintessential EoS $\omega_{DE} > -1$ diminishing at late time ($z < 5$) to $\omega_{DE}|_{z=0} \simeq -0.724$. This behavior differs from variable EoS in other $F(R)$ models [36–38], where $\omega_{DE}(z)$ for the best fitted solutions evolve from a phantom to a quintessential stage at $z < 2$.

Note that the normalized Hubble parameter $E(x)$ for the $F(R, \phi)$ model (2.2), (2.8) in the top-left panel of Fig. 1 exceeds the Λ CDM $E(x)$ at high redshifts or $x \rightarrow -\infty$. This difference is an inevitable feature of the $F(R, \phi)$ model, and the best description of the observations is achieved when this difference is minimal. The evolution of the scalar field rate parameter (2.12) $\Psi = \kappa \dot{\phi}/H_0$ looking like the straight line in the bottom-left panel of Fig. 1 shows that it behaves approximately as $\Psi \simeq \Psi_0 a^{-3}$. In other words, the last term $3A\Omega_\Lambda \mathcal{R}^n/E$ in the right hand side of Eq. (2.17) appeared to be vanishing for the best fit parameters.

III. GENERALIZED EXPONENTIAL $F(R)$ MODEL

The generalized exponential $F(R)$ model with the Lagrangian,

$$F(R) = R + \frac{R^2}{M^2} - \Lambda \left[2 - \alpha \exp \left(-\beta \frac{R}{2\Lambda} \right) \right]. \quad (3.1)$$

was considered in Ref. [37]. Here α and β are positive constants, $F_{\text{inf}}(R) = \frac{R^2}{M^2}$ is the inflationary term, it is assumed to be negligible near and after the recombination epoch. This model has the Λ CDM-like asymptotic behavior at the large R limit, in other words, its Lagrangian tends to the Λ CDM expression $F(R) \approx R - 2\Lambda$ at the epoch, when $R \gg \Lambda$, but far later the inflationary era, where $F_{\text{inf}}(R)$ remains negligible.

The dynamics of the model (3.1) and other scenarios with similar asymptotic behavior was described in Refs. [37, 38] and it reduces to the relation (2.10) $R = 6\dot{H} + 12H^2$ and the Friedmann equation

$$\frac{dR}{d \log a} = \frac{1}{F''(R)} \left(\frac{\kappa^2 \rho}{3H^2} - F'(R) + \frac{RF'(R) - F}{6H^2} \right). \quad (3.2)$$

These equations in the notation of Eq. (2.12) may be reduced to the system including Eq. (2.14) and the equation,

$$\frac{d\mathcal{R}}{dx} = 2 \frac{[\Omega_m^0 (a^{-3} + X_r a^{-4}) + \Omega_\Lambda (1 - \frac{1}{2} \alpha (1 + \beta \mathcal{R}) e^{-\beta \mathcal{R}})] / E^2 - 1 + \frac{1}{2} \alpha \beta e^{-\beta \mathcal{R}}}{\alpha \beta^2 e^{-\beta \mathcal{R}}}. \quad (3.3)$$

This system should be integrated numerically, but unlike the $F(R, \phi)$ model (2.2), in this scenario only the future direction for integrating is acceptable (with growing a or x), because in the opposite direction the integral curves of the system (2.14), (3.3) diverge and deviate from viable solutions. Hence, we can not start from the present time and have to define initial conditions for the system (2.14), (3.3) at some point a_{ini} or equivalently $z_{\text{ini}} = a_{\text{ini}}^{-1} - 1$ in the past. This initial point for the considered model (3.1) is determined from the condition that the term $F''(R)$ in the denominator of Eq.(3.2) should be very small, but not negligible. More precisely, the dimensionless factor $\delta = \alpha \beta^2 e^{-\beta \mathcal{R}_{\text{ini}}}$ in the denominator of Eq.(3.3) should be much smaller than unity.

At the initial point a_{ini} and before, the solutions $H(a)$, $\mathcal{R}(a)$ of the $F(R)$ model (3.1) should have the Λ CDM-like asymptotic behavior (2.20) [36–38]:

$$\frac{H^2}{H_0^2} = \Omega_m^0 (a^{-3} + X_r a^{-4}) + \Omega_\Lambda, \quad \mathcal{R} = \frac{R}{2\Lambda} = 2 + \frac{\Omega_m^0}{2\Omega_\Lambda} a^{-3}. \quad (3.4)$$

To determine a_{ini} we assume $\delta \sim 10^{-9}$ and obtain,

$$a_{\text{ini}} = \left[\frac{2\Omega_\Lambda}{\Omega_m^0} \left(\frac{\log(\alpha\beta^2/\delta)}{\beta} - 2 \right) \right]^{-1/3}. \quad (3.5)$$

During integration of the system (2.14), (3.3), we should also solve another problem: at the starting point a_{ini} we do not know the true value of the Hubble constant H_0 and therefore the parameters $\Omega_m^0, \Omega_\Lambda$ are unknown. Following Refs. [36–38] we introduce a “preliminary” Λ CDM-asymptotical Hubble constant H_0^* at the initial point, that differs from the true Hubble constant $H_0 = H(t_0)$ achieved during evolution in this scenario from a_{ini} to the present day value $a = 1$. The value H_0^* determines the normalized Hubble rate,

$$E^* = \frac{H}{H_0^*}, \quad (3.6)$$

and also the parameters,

$$\Omega_m^* = \frac{\kappa^2 \rho_m^0}{(H_0^*)^2}, \quad \Omega_\Lambda^* = \frac{\Lambda}{3(H_0^*)^2}. \quad (3.7)$$

When we integrate the system with the modified equation (2.14),

$$\frac{dE^*}{dx} = \Omega_\Lambda^* \frac{\mathcal{R}}{E^*} - 2E^*, \quad (3.8)$$

and Eq. (3.3), with $\Omega_m^0/E^2 = \Omega_m^*/(E^*)^2$ and $\Omega_\Lambda/E^2 = \Omega_\Lambda^*/(E^*)^2$, we obtain the solution $E^*(a)$, leading to the Hubble parameter $H(a) = H_0^* E^*(a)$. Thus we reconstruct the Hubble constant $H_0 = H|_{a=1} = H_0^* E^*|_{a=1}$ and the parameters $\Omega_m^0, \Omega_\Lambda$ from the relations,

$$\Omega_m^0 H_0^2 = \Omega_m^* (H_0^*)^2 = \kappa^2 \rho_m^0, \quad \Omega_\Lambda H_0^2 = \Omega_\Lambda^* (H_0^*)^2 = \frac{\Lambda}{3}, \quad \frac{\Omega_\Lambda}{\Omega_m^0} = \frac{\Omega_\Lambda^*}{\Omega_m^*}. \quad (3.9)$$

These solutions are shown in Fig. 1 and are tested with the observational data.

IV. OBSERVATIONAL DATA TESTS

We now describe the process of using and interpreting the observational data, by using the line of research developed in previous studies [36–38]. For the Pantheon+ catalog [3] of Type Ia supernovae (SNe Ia) data with $N_{\text{SN}} = 1701$ datapoints of the distance moduli μ_i^{obs} at redshifts z_i we calculate the χ^2 function:

$$\chi_{\text{SN}}^2(\theta_1, \dots) = \min_{H_0} \sum_{i,j=1}^{N_{\text{SN}}} \Delta\mu_i (C_{\text{SN}}^{-1})_{ij} \Delta\mu_j, \quad \Delta\mu_i = \mu^{\text{th}}(z_i, \theta_1, \dots) - \mu_i^{\text{obs}}. \quad (4.1)$$

Here C_{SN} is the covariance matrix [3] and the theoretical estimates of the distance moduli are made as follows,

$$\mu^{\text{th}}(z) = 5 \log_{10} \frac{(1+z) D_M(z)}{10 \text{pc}}, \quad D_M(z) = c \int_0^z \frac{d\tilde{z}}{H(\tilde{z})}. \quad (4.2)$$

For baryon acoustic oscillations data from the DESI 2025 [2], we calculate the values,

$$\frac{D_M(z)}{r_d}, \quad \frac{D_H(z)}{r_d} = \frac{c}{H(z) r_d}, \quad \frac{D_V(z)}{r_d} = \frac{(z D_H D_M^2)^{1/3}}{r_d},$$

where $r_d = r_s(z_d)$ is THE comoving sound horizon at the end of the baryon drag era, calculated in accordance with Refs. [36–38] as the integral,

$$r_s(z) = \int_z^\infty \frac{c_s(\tilde{z})}{H(\tilde{z})} d\tilde{z} = \frac{1}{\sqrt{3}} \int_0^{1/(1+z)} \frac{da}{a^2 H(a) \sqrt{1 + [3\Omega_b^0 / (4\Omega_\gamma^0)] a}}, \quad (4.3)$$

We use BAO DESI data [2] with the observed value $D_V(z_1)/r_d$ at $z_1 = 0.295$ and data points with $D_M(z_i)/r_d$ and $D_H(z_i)/r_d$ for higher redshifts z_i and we calculate the χ^2 function,

$$\chi_{\text{BAO}}^2(\theta_1, \dots) = \left[\frac{\Delta_V(z_1)}{\sigma_V(z_1)} \right]^2 + \sum_{i=2}^8 [\Delta_M(z_i) \ \Delta_H(z_i)] C_{M,H}^i \begin{bmatrix} \Delta_M(z_i) \\ \Delta_H(z_i) \end{bmatrix}, \quad (4.4)$$

where, $\Delta_q = \left(\frac{D_q}{r_d}\right)^{\text{th}} - \left(\frac{D_q}{r_d}\right)^{\text{obs}}$, $q = V, M, H$; $C_{M,H}^i$ are the covariance matrices with the errors $\sigma_q(z_1)$ and the cross-correlation coefficients $r_{M,H}^i$ between $D_M(z_i)/r_d$ and $D_H(z_i)/r_d$.

For the Hubble parameter data $H(z)$ we use here $N_H = 34$ datapoints of $H^{\text{obs}}(z_i)$ (Cosmic Chronometers) tabulated in Ref. [31] and we calculate the corresponding χ^2 function,

$$\chi_H^2 = \sum_{i=1}^{N_H} \left[\frac{H^{\text{obs}}(z_i) - H^{\text{th}}(z_i; \theta_k)}{\sigma_{H,i}} \right]^2. \quad (4.5)$$

To determine the best fit model parameters of the considered scenarios, we calculate and minimize the total χ^2 function with the contributions from SNe Ia (4.1), BAO DESI (4.4) and the Hubble parameter data (4.5):

$$\chi^2 = \chi_{\text{SN}}^2 + \chi_{\text{BAO}}^2 + \chi_H^2. \quad (4.6)$$

The results of these calculations for the $F(R, \phi)$ model (2.2), (2.8) in comparison to the Λ CDM scenario (2.20) and the generalized exponential $F(R)$ model (3.1) are presented in Table IV and in Fig. 2. One can see that the $F(R, \phi)$ model describes this data more successfully than the Λ CDM, not only in the achieved value of $\min \chi^2$ (2008.43 vs 2037.79), but also after consideration of the Akaike information criterion (AIC) [77]

$$\text{AIC} = \min \chi^2 + 2N_p. \quad (4.7)$$

Here N_p is the number of free model parameters: $N_p = 7$ (see (2.19)) for the model (2.2), (2.8) and $N_p = 2$ for the Λ CDM scenario (2.20). This criterion brings an additional advantage to scenarios with small number N_p , but this advantage appeared to be insufficient to change the resulting physical picture. Fig. 2 illustrates our analysis of the χ^2 function (4.6) for the $F(R, \phi)$ model with contour plots at 1σ ,

TABLE I. Best fits with 1σ errors, $\min \chi^2$, AIC, from SNe Ia, BAO DESI and $H(z)$ data, for the $F(R, \phi)$ model (2.2), (2.8) in comparison with the Λ CDM model (2.20) and the generalized exponential $F(R)$ model (3.1).

Model	$\min \chi^2 / d.o.f$	AIC	Ω_m^0	H_0	other parameters
$F(R, \phi)$	2008.43 / 1736	2022.43	$0.2406^{+0.0198}_{-0.0128}$	$66.39^{+1.39}_{-1.40}$	$n = 1.53^{+0.033}_{-0.021}$, $A = 0.0098^{+0.0024}_{-0.0014}$, $\mathcal{R}_0 = 1.74^{+0.06}_{-0.11}$, $\Psi_0 = 1.615^{+0.045}_{-0.093}$, $\Phi_0 = -6340^{+68}_{-74}$
Λ CDM	2037.79 / 1741	2041.79	$0.2998^{+0.0027}_{-0.0028}$	$69.01^{+1.61}_{-1.54}$	-
Exp $F(R)$	2008.18 / 1738	2018.18	$0.3213^{+0.0065}_{-0.0052}$	$66.46^{+1.60}_{-1.60}$	$\alpha = 2.76^{+3.34}_{-1.42}$, $\beta = 0.694^{+0.196}_{-0.237}$, $\Omega_\Lambda = 0.545^{+0.062}_{-0.074}$

2σ confidence levels (CL) for two-parameter distributions $\chi^2(\theta_j, \theta_k)$ with pairs of free parameters (2.19). For each pair of chosen model parameters to calculate $\chi^2(\theta_j, \theta_k)$ we seek for the minimum of χ^2 over the remaining five parameters. In this process, the grid spacing and the size of the box for other parameters are determined at the initial stage, but the center of the box is approximated during this process. The prior ranges for the model parameters have their physical limits, in particular, for the $F(R, \phi)$ model (2.2), (2.8) they are,

$$\Omega_m^0 \in [0.05, 0.5]; \quad n \in (1, 2]; \quad A \in [0, 1]; \quad \mathcal{R}_0 \in [0.5, 5]; \quad \Phi_0 \in [-10^5, -50]; \quad \Psi_0 \in [0, 5]; \quad H_0 H_0 \in [50, 100] \frac{\text{km}}{\text{s} \cdot \text{Mpc}}. \quad (4.8)$$

In the top-right panel in Fig. 2 one-parameter distributions are presented, with,

$$\chi^2(H_0) = \min_{\text{other } \theta_j} \chi^2(\theta_1, \theta_2, \dots, H_0).$$

for the aforementioned three models. One can see that the $F(R, \phi)$ and $F(R)$ models (2.2), (3.1) are much more successful regarding the minimum of χ^2 , which is essentially lower than the Λ CDM model. The estimates of $\min \chi^2$ in Table IV show the difference $\Delta \min \chi^2$ of order 30 in favor of the $F(R, \phi)$ and

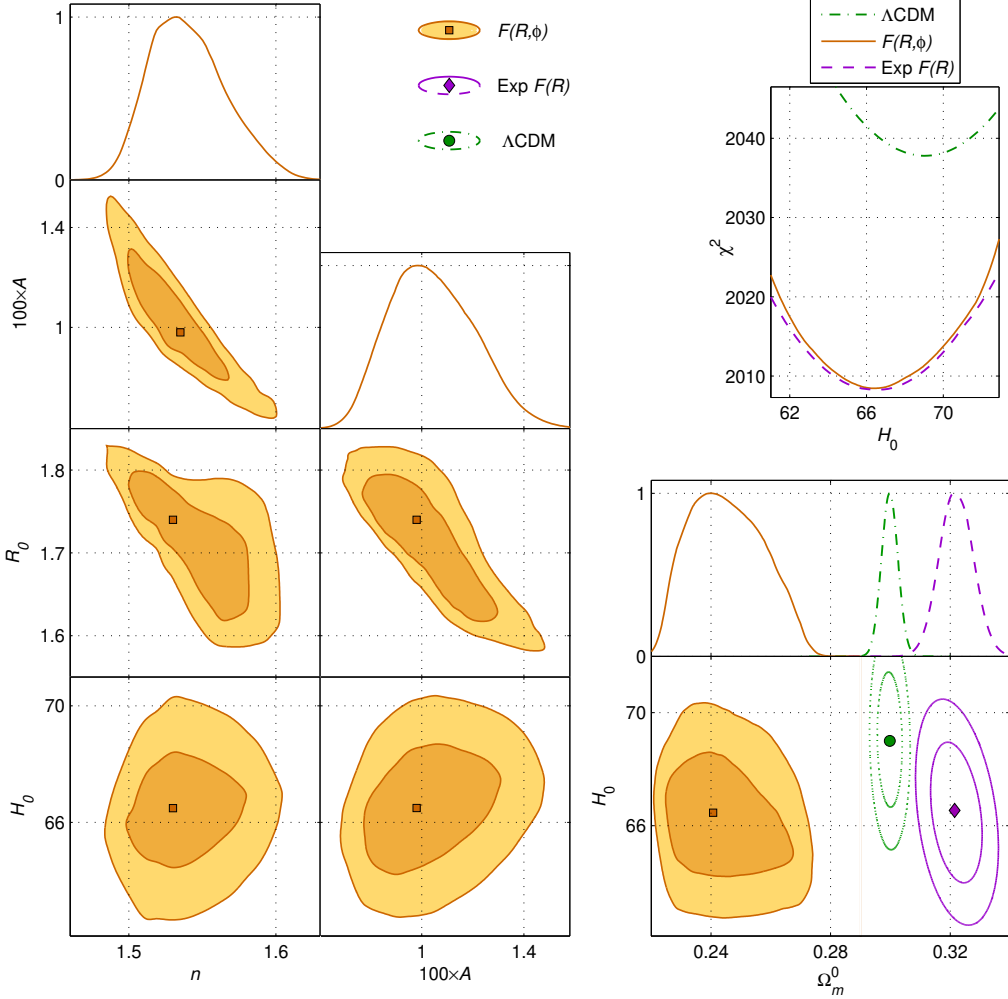


FIG. 2. Contour plots of χ^2 with 1σ , 2σ CL, likelihood functions $\mathcal{L}(\theta_i)$ and one-parameter distributions $\chi^2(H_0)$ for the $F(R, \phi)$ model (2.2), (2.8) in comparison with the Λ CDM model (2.20) and the $F(R)$ model (3.1) for SNe Ia, BAO DESI and $H(z)$ data.

$F(R)$ models. This advantage is kept also for the Akaike information criterion: $\Delta\text{AIC} \simeq -19.36$ for the $F(R, \phi)$ and $\Delta\text{AIC} \simeq -23.61$ for the $F(R)$ model.

The likelihood functions $\mathcal{L}(\theta_j)$ for the parameters θ_j shown in Fig. 2 are related with the corresponding one-parameter distributions $\chi^2(\theta_j)$:

$$\mathcal{L}(\theta_j) = \exp \left[-\frac{\chi^2(\theta_j) - m_{\text{abs}}}{2} \right], \quad (4.9)$$

where m_{abs} is the absolute minimum for χ^2 . The squares for the $F(R, \phi)$ models, circles and diamonds for other models, denote the best fits with $\min \chi^2$ of the corresponding $\chi^2(\theta_j, \theta_k)$. We see that the best fits for the exponent n lie in the narrow range $1.5 < n < 1.6$, the best fit for A is of order 0.01, suitable interval for Φ_0 is negative: $\Phi_0 = -6340_{-74}^{+68}$.

In the bottom-right panel of Fig. 2 with contours in the $\Omega_m^0 - H_0$ plane we compare the $F(R, \phi)$ model (2.2), (2.8) with two other models. One may conclude that the best Ω_m^0 fits for the $F(R, \phi)$ model are essentially lower compared to other scenarios. This difference may be related with the different physical significance of Ω_m^0 and of dark energy in these scenarios. The similar analysis of observational tests with SNe Ia, BAO DESI and $H(z)$ data for the generalized exponential $F(R)$ model (3.1) is illustrated in Fig. 3. This model is the most successful in $\min \chi^2$ and AIC having $N_p = 5$ parameters, though the resulting χ^2 in this case, is close to that of the $F(R, \phi)$ model. The prior ranges for the scenario (3.1) coincide with (4.8) for Ω_m^0 and H_0 and $\alpha \in [0, 30]$; $\beta \in [0, 10]$; $\Omega_\Lambda \in [0.4, 1]$.

In the $\Omega_m^0 - H_0$ plane, the difference between the best fits for Ω_m^0 exceeds 3σ : it can explain the advantage in $\min \chi^2$ over the Λ CDM model for the chosen set of observational data. This success of the $F(R)$ scenario is also connected with behavior of its effective dark energy EoS parameter $\omega_{DE}(z)$ (2.21) at redshift $0 < z < 3$ shown in Fig. 1. As one can see, $\omega_{DE}(z)$ evolves from a phantom to a quintessence

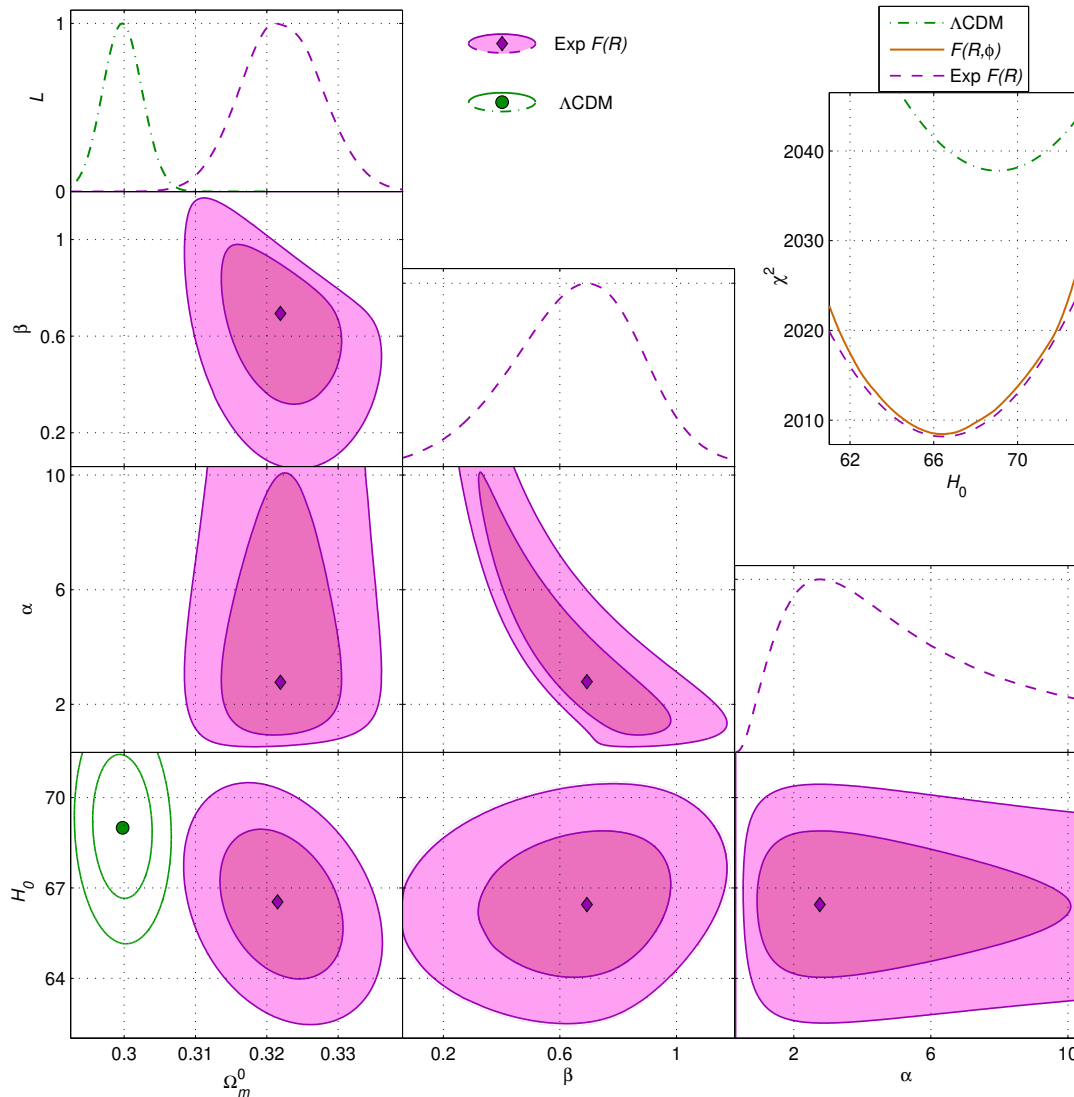


FIG. 3. Contour plots of χ^2 with 1σ , 2σ CL, likelihood functions $\mathcal{L}(\theta_i)$ and one-parameter distributions $\chi^2(H_0)$ for the generalized exponential $F(R)$ model (3.1) in comparison with models (2.2) and (2.20) for SNe Ia, BAO DESI and $H(z)$ data.

stage. The difference in the best fits for H_0 between the $F(R)$ and Λ CDM models is not so striking, but also essential, since the considered $F(R, \phi)$ and $F(R)$ models predict the Hubble constant H_0 of the order 66.4 km/s/Mpc. The 2σ CL domains for the parameters α and β are extended to larger $\alpha > 10$ and small $\beta \sim 0.05$. These features depend on chosen observational datasets, and in the next section we will see how this picture changes with the addition of the CMB data in our statistical analysis.

V. OBSERVATIONAL TESTS WITH THE ADDITION OF CMB DATA

The considered $F(R, \phi)$ model (2.2), (2.8) and other scenarios should be also confronted with observational data coming from the CMB. In this article, we use the CMB observational parameters in accordance with Refs. [36–38]

$$\mathbf{x} = (R, \ell_A, \omega_b), \quad R = \sqrt{\Omega_m^0} \frac{H_0 D_M(z_*)}{c}, \quad \ell_A = \frac{\pi D_M(z_*)}{r_s(z_*)}, \quad \omega_b = \Omega_b^0 h^2$$

with the Planck 2018 data priors [10, 78]

$$\mathbf{x}^{\text{Pl}} = (R^{\text{Pl}}, \ell_A^{\text{Pl}}, \omega_b^{\text{Pl}}) = (1.7428 \pm 0.0053, 301.406 \pm 0.090, 0.02259 \pm 0.00017)$$

for scenarios with zero spatial curvature. Here, the comoving sound horizon $r_s(z_*)$ is calculated as the integral (4.3) where the redshift $z_* \simeq 1090$ is related to the photon-decoupling epoch. The value

z_* is estimated following Refs. [36, 59, 78]. We calculate the χ^2 function with the covariance matrix $C_{\text{CMB}} = \|\tilde{C}_{ij}\sigma_i\sigma_j\|$ [78]

$$\chi_{\text{CMB}}^2 = \min_{\omega_b, H_0} \Delta \mathbf{x} \cdot C_{\text{CMB}}^{-1} (\Delta \mathbf{x})^T, \quad \Delta \mathbf{x} = \mathbf{x} - \mathbf{x}^{\text{Pl}}.$$

and the total χ^2 with the following four sources of observational data,

$$\chi_{\text{tot}}^2 = \chi_{\text{SN}}^2 + \chi_{\text{BAO}}^2 + \chi_H^2 + \chi_{\text{CMB}}^2. \quad (5.1)$$

Calculations of χ_{tot}^2 including the CMB data for the $F(R, \phi)$ model (2.2), (2.8) led to rather disappointing results, since the values χ_{tot}^2 appeared to be extremely large. These results are directly related with the behavior of $F(R, \phi)$ solutions shown in Fig. 1; if the chosen model parameters (2.19) satisfy the SNe Ia, BAO DESI and $H(z)$ CC limitations, the resulting normalized Hubble rate $E(z)$ at $z \sim 1000$ (or $a \sim 10^{-3}$) essentially exceeds $E(z)$ for the Λ CDM and generalized exponential models. This behavior allows us to describe BAO DESI data with some difficulty because of the integral (4.3) for r_d , but it becomes an overpowering obstacle after including the CMB data related to $z \sim 1100$.

From another side, we can describe the CMB data with the $F(R, \phi)$ model (2.2), (2.8) successfully if we choose the starting point a_{ini} for the integration near $a \sim 10^{-3}$. But in this case the SNe Ia, BAO DESI and CC data related to $z \in [0, 2.4]$ appear to be described badly with large χ^2 (4.6). One may conclude that the $F(R, \phi)$ model (2.2), (2.8) needs some corrections for successful tests with all considered observational data.

The generalized exponential $F(R)$ (3.1) and Λ CDM (2.20) models appear to be more appropriate in confrontation with all the SNe Ia, BAO DESI, CC and CMB data. The results of the test with χ_{tot}^2 function (5.1) are presented in Table V and Fig. 4. These calculations support the results of Ref. [37], but with the renewed approach for BAO DESI DR2 data [2] and 34 $H(z)$ CC datapoints from Ref. [31]. From these calculations we can draw the main conclusion: if we add the CMB observational data,

TABLE II. Best fits with 1σ errors, $\min \chi^2$, AIC, from SNe Ia, BAO DESI, $H(z)$ CC and CMB data, for the generalized exponential $F(R)$ model (3.1) and the Λ CDM model (2.20).

Model	$\min \chi^2/d.o.f$	AIC	Ω_m^0	H_0	other parameters
Exp $F(R)$	2019.04 /1741	2029.04	$0.3179_{-0.0053}^{+0.0056}$	$65.10_{-1.54}^{+1.55}$	$\alpha = 0.865_{-0.282}^{+0.480}$, $\beta = 0.807_{-0.082}^{+0.104}$, $\Omega_\Lambda = 0.662_{-0.082}^{+0.073}$
Λ CDM	2048.71 /1744	2052.71	$0.2923_{-0.0011}^{+0.0011}$	$67.62_{-1.53}^{+1.52}$	-

the large advantage of the $F(R)$ scenario over the Λ CDM model is conserved in $\min \chi_{\text{tot}}^2$ and in AIC: $\Delta \min \chi_{\text{tot}}^2 \simeq -29.67$ and $\Delta \text{AIC} \simeq -23.67$ in favor of the $F(R)$ model. Hence, this advantage is not connected with CMB, but with BAO DESI along with SNe Ia observational data related to $z \in [0, 3]$, where in the $F(R)$ model the dark energy EoS parameter $\omega_{DE}(z)$ (2.21) evolves from a phantom to a quintessence stage. The bottom-left panel of Fig. 4 with the $\Omega_m^0 - H_0$ plane demonstrates that the additional CMB data slightly diminishes the best fits both for Ω_m^0 and H_0 for both models. But the most essential changes can be seen for the best fits of α : they change from $\alpha = 2.76_{-1.42}^{+3.34}$ for χ^2 to $\alpha = 0.865_{-0.282}^{+0.48}$ for χ_{tot}^2 . To unify contour plots for both cases we use the logarithmic scale α in the corresponding planes in Fig. 4. The best fits for β with the CMB data are slightly enhanced, but the error boxes and 1σ , 2σ CL domains become noticeably more narrow. Note that the Lagrangian (3.1) of the generalized exponential $F(R)$ model in the limit $\beta \rightarrow \infty$ tends to the Λ CDM Lagrangian $F(R) = R - 2\Lambda$. The best fitted values $\beta = 0.807_{-0.082}^{+0.104}$ are low, hence the considered exponential $F(R)$ model works far from its Λ CDM limit.

VI. CONCLUSIONS

In this article, we explored the $F(R, \phi)$ scenario (2.2), (2.8) originated from the ghost-free non-local gravity in comparison with the generalized exponential $F(R)$ model (3.1) and the Λ CDM model. To determine a late-time evolution of the $F(R, \phi)$ model, we solved the system of equations (2.14)–(2.17) starting from the initial conditions at the present time $t = t_0$ and integrating to the past time direction. This feature is the essential advantage of this scenario, because the mentioned approach is not acceptable for the $F(R)$ model (3.1) and many others $F(R)$ scenarios [36–38], where integral curves sharply diverge if we integrate into the past time direction. These models require another approach.

Viable solutions of the $F(R, \phi)$ model were confronted with the observational data including the Pantheon+ Type Ia supernovae (SNe Ia), the DESI DR2 measurements of BAO and the Hubble parameter estimations $H(z)$ (Cosmic Chronometers). The $F(R, \phi)$ scenario appeared to be rather successful: its

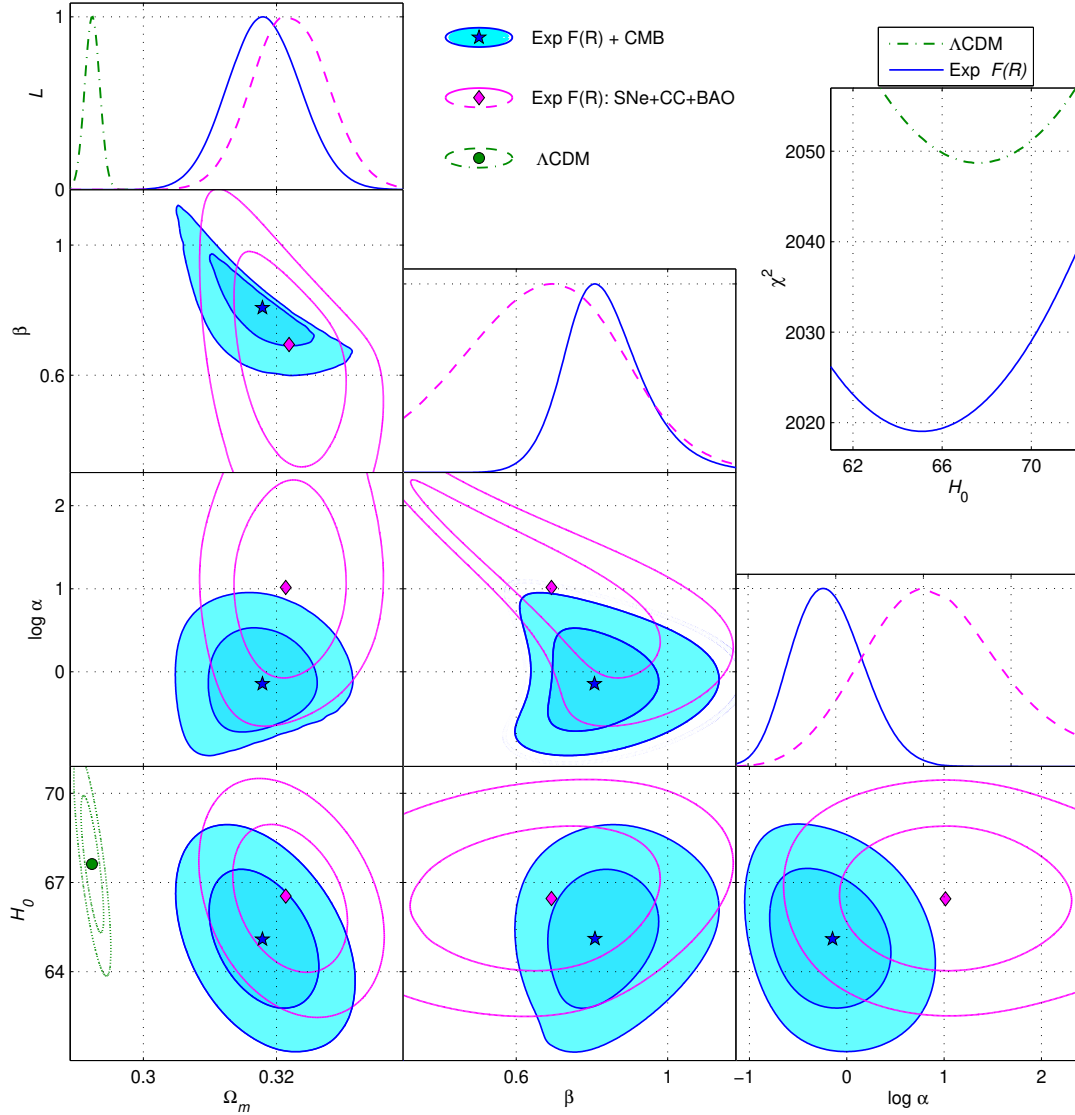


FIG. 4. Contour plots of χ_{tot}^2 , likelihoods $\mathcal{L}(\theta_i)$ distributions $\chi_{\text{tot}}^2(H_0)$ for the generalized exponential $F(R)$ model (3.1) for SNe Ia, BAO DESI, $H(z)$ CC and CMB data in comparison with Λ CDM model and the χ^2 function (4.6).

$\min \chi^2$ is comparable with that of the generalized exponential $F(R)$ model and essentially exceeds the Λ CDM result. This large advantage is kept if we use the Akaike information criterion, taking into account the number N_p of free model parameters, though the $F(R, \phi)$ model has the large number $N_p = 7$ in contrast to $N_p = 2$ of the Λ CDM model.

However, if we add the CMB observed parameters to the mentioned observational data, the $F(R, \phi)$ model encounters serious difficulties. The total χ_{tot}^2 function (5.1) appears to be large, because the CMB data are related with the recombination epoch at redshifts $z \sim 1100$ and at these redshifts this model has too large normalized Hubble rate $E(z)$ (shown in Fig. 1) for the best fitted solutions with respect to SNe Ia, BAO DESI and CC data related to $z \in [0, 3]$. We can not bypass this difficulty if we start our calculations from $z \sim 1000$ epoch and the CMB data. So we may conclude that the $F(R, \phi)$ model (2.2), (2.8) needs some modifications or correction terms to describe all the observational data including CMB.

On the other hand, the generalized exponential $F(R)$ model (3.1) is very successful in tests with the whole set of Pantheon+ SNe Ia, DESI BAO, $H(z)$ and CMB data. When we include the CMB data, the best fits for its parameters α and β noticeably change as can be seen in Fig. 4. However, if we add the CMB observational data, the large advantage of the $F(R)$ scenario over the Λ CDM model is conserved, in particular, for SNe Ia, BAO and $H(z)$ data we observe the difference $\Delta \min \chi^2 \simeq -29.61$ between these models and with CMB data the difference is $\Delta \min \chi_{\text{tot}}^2 \simeq -29.67$ in favor of the $F(R)$ model. The same picture is seen if we compare AIC values.

From this fact we conclude that the large advantage of the generalized exponential $F(R)$ scenario over the Λ CDM model does not depend on CMB, but is connected with BAO DESI along with SNe Ia

observational data related to $z \in [0, 3]$. One can see in Fig. 1 that the dark energy EoS parameter $\omega_{DE}(z)$ (2.21) of the $F(R)$ model evolves from a phantom to a quintessence stage at these redshifts. Such a form of dynamical effective dark energy is observed in other successful $F(R)$ scenarios [36–38], whereas for the $F(R, \phi)$ model (2.2), (2.8) we see only a quintessence behavior with $\omega_{DE}(z) > -1$. This conclusion is somewhat decisive that not all modified gravity models can successfully be compatible with all the data, and points out the elevated role of $F(R)$ gravity, among all the modified gravities; it also signifies its fundamental importance as a complete theory of gravity.

ACKNOWLEDGMENTS

-
- [1] A. G. Adame *et al.* [DESI], JCAP **02** (2025), 021, [arXiv:2404.03002 [astro-ph.CO]].
- [2] M. Abdul Karim *et al.* [DESI], Phys. Rev. D **112** (2025) no.8, 083515, [arXiv:2503.14738 [astro-ph.CO]].
- [3] D. Scolnic *et al.*, Astrophys. J. **938** (2022) 113, arXiv:2112.03863.
- [4] D. Rubin *et al.*, Astrophys. J. **986** (2025) no.2, 231, arXiv:2311.12098 [astro-ph.CO].
- [5] T. M. C. Abbott *et al.* (DES), Astrophys. J. Lett. **973**, no.1 L14 (2024), arXiv:2401.02929 [astro-ph.CO].
- [6] P. J. E. Peebles and B. Ratra, Rev. Mod. Phys. **75**, 559 (2003), arXiv:astro-ph/0207347.
- [7] K. Bamba, S. Capozziello, S. Nojiri and S. D. Odintsov, Astrophys. Space Sci. **342** (2012), 155-228, [arXiv:1205.3421 [gr-qc]].
- [8] S. Capozziello, M. De Laurentis, Phys. Rept. **509**, 167 (2011);
V. Faraoni and S. Capozziello, Fundam. Theor. Phys. **170** (2010)
- [9] S. Nojiri, S.D. Odintsov, [Int. J. Geom. Meth. Mod. Phys. **4**, 115 (2007)], [arXiv:hep-th/0601213];
S. Nojiri, S.D. Odintsov, Phys. Rept. **505**, 59 (2011), [arXiv:1011.0544 [gr-qc]];
- S. Nojiri, S. D. Odintsov and V. K. Oikonomou, Phys. Rept. **692** (2017) 1 [arXiv:1705.11098 [gr-qc]].
- [10] Planck collaboration: N. Aghanim *et al.*, Astron. Astrophys. **641** (2020), A6 [arXiv:1807.06209 [astro-ph.CO]].
- [11] A.G. Riess, W. Yuan, L.M. Macri and D. Scolnic, Astrophys. J. Lett. **908** (2021), L6, arXiv:2112.04510 [astro-ph.CO].
- [12] E. Di Valentino, A. Mukherjee and A. A. Sen, Entropy **23** (2021) no.4, 404 doi:10.3390/e23040404 [arXiv:2005.12587 [astro-ph.CO]].
- [13] E. Di Valentino, S. Gariazzo, O. Mena and S. Vagnozzi, JCAP **07** (2020) no.07, 045. [arXiv:2005.02062[astro-ph.CO]].
- [14] C. Krishnan, E. Ó. Colgáin, Ruchika, A. A. Sen, M. M. Sheikh-Jabbari and T. Yang, Phys. Rev. D **102** (2020) no.10, 103525 [arXiv:2002.06044 [astro-ph.CO]].
- [15] C. Krishnan, R. Mohayaee, E. Ó. Colgáin, M. M. Sheikh-Jabbari and L. Yin, Class. Quant. Grav. **38** (2021) no.18, 184001 doi:10.1088/1361-6382/ac1a81 [arXiv:2105.09790 [astro-ph.CO]].
- [16] S. D. Odintsov, D. Sáez-Chillón Gómez and G. S. Sharov, Nucl. Phys. B. **966**, (2021), 115377, arXiv:2011.03957.
- [17] S. Vagnozzi, L. Visinelli, P. Brax, A. C. Davis and J. Sakstein, Phys. Rev. D **104** (2021) no.6, 063023, [arXiv:2103.15834 [hep-ph]].
- [18] S. Vagnozzi, F. Pacucci and A. Loeb, JHEAp **36** (2022), 27-35, [arXiv:2105.10421 astro-ph.CO]].
- [19] G. Ye, J. Zhang and Y. S. Piao, [arXiv:2107.13391 [astro-ph.CO]].
- [20] F. Ferlito, S. Vagnozzi, D. F. Mota and M. Baldi, Mon. Not. Roy. Astron. Soc. **512** (2022) no.2, 1885-1905, [arXiv:2201.04528 [astro-ph.CO]].
- [21] B. H. Lee, W. Lee, E. Ó. Colgáin, M. M. Sheikh-Jabbari and S. Thakur, JCAP **04** (2022) no.04, 004, [arXiv:2202.03906 [astro-ph.CO]].
- [22] S. A. Adil, U. Mukhopadhyay, A. A. Sen and S. Vagnozzi, JCAP **10** (2023), 072, [arXiv:2307.12763 [astro-ph.CO]].
- [23] M. Högås and E. Mörtsell, Phys. Rev. D **108** (2023) no.12, 124050 doi:10.1103/PhysRevD.108.124050 [arXiv:2309.01744 [astro-ph.CO]].
- [24] N. Menci, S. A. Adil, U. Mukhopadhyay, A. A. Sen and S. Vagnozzi, JCAP **07** (2024), 072, [arXiv:2401.12659 [astro-ph.CO]].
- [25] E. Di Valentino, J. Levi Said, A. Riess, A. Pollo, V. Poulin, A. Gómez-Valent, A. Weltman, A. Palmese, C. D. Huang and C. van de Bruck, *et al.* [arXiv:2504.01669 [astro-ph.CO]].
- [26] Y. Cai, X. Ren, T. Qiu, M. Li and X. Zhang, [arXiv:2505.24732 [astro-ph.CO]].
- [27] G. Ye, M. Martinelli, B. Hu and A. Silvestri, Phys. Rev. Lett. **134** (2025) no.18, 181002, [arXiv:2407.15832 [astro-ph.CO]].
- [28] H. Chaudhary, S. Capozziello, V. K. Sharma, I. Gómez-Vargas and G. Mustafa, [arXiv:2508.10514 [astro-ph.CO]].
- [29] H. Chaudhary, S. Capozziello, S. Prahara, S. K. J. Pacif and G. Mustafa, JHEAp **50** (2026), 100507, [arXiv:2509.17124[gr-qc]].

- [30] W. Giarè, M. A. Sabogal, R. C. Nunes and E. Di Valentino, *Phys. Rev. Lett.* **133** (2024) no.25, 251003, [arXiv:2404.15232 [astro-ph.CO]].
- [31] S. Pan, S. Paul, E. N. Saridakis and W. Yang, *Phys. Rev. D* **113** (2026) no.2, 023515, [arXiv:2504.00994[astro-ph.CO]].
- [32] Y. Yang, Q. Wang, X. Ren, E. N. Saridakis and Y. F. Cai, *Astrophys. J.* **988** (2025) no.1, 123 doi:10.3847/1538-4357/ade43f [arXiv:2504.06784 [astro-ph.CO]].
- [33] X. Zhang, Y. H. Xu and Y. Sang, *Commun. Theor. Phys.* **78** (2026) no.3, 035404 doi:10.1088/1572-9494/ae1a5b [arXiv:2511.02220 [astro-ph.CO]].
- [34] D. D. Y. Ong, D. Yallup and W. Handley, [arXiv:2511.10631 [astro-ph.CO]].
- [35] S. Nojiri, S. D. Odintsov and V. K. Oikonomou, [arXiv:2512.06279 [gr-qc]].
- [36] S. D. Odintsov, D. Sáez-Chillón Gómez and G. S. Sharov, *Eur. Phys. J. C* **85** (2025) no.3, 298, [arXiv:2412.09409 [gr-qc]].
- [37] S. D. Odintsov, V. K. Oikonomou and G. S. Sharov, *JHEAp* **50** (2026), 100471, [arXiv:2506.02245[gr-qc]].
- [38] S. D. Odintsov, V. K. Oikonomou and G. S. Sharov, *JHEAp* **52** (2026), 100579, [arXiv:2601.06949[gr-qc]].
- [39] S. Nojiri and S. D. Odintsov, *Phys. Rev. D* **68** (2003), 123512, [arXiv:hep-th/0307288 [hep-th]].
- [40] S. Capozziello, V. F. Cardone and A. Troisi, *Phys. Rev. D* **71** (2005), 043503, [arXiv:astro-ph/0501426[astro-ph]].
- [41] J. c. Hwang and H. Noh, *Phys. Lett. B* **506** (2001), 13-19 doi:10.1016/S0370-2693(01)00404-X [arXiv:astro-ph/0102423 [astro-ph]].
- [42] Y. S. Song, W. Hu and I. Sawicki, *Phys. Rev. D* **75** (2007), 044004 doi:10.1103/PhysRevD.75.044004 [arXiv:astro-ph/0610532 [astro-ph]].
- [43] T. Faulkner, M. Tegmark, E. F. Bunn and Y. Mao, *Phys. Rev. D* **76** (2007), 063505 doi:10.1103/PhysRevD.76.063505 [arXiv:astro-ph/0612569 [astro-ph]].
- [44] G. J. Olmo, *Phys. Rev. D* **75** (2007), 023511 doi:10.1103/PhysRevD.75.023511 [arXiv:gr-qc/0612047 [gr-qc]].
- [45] I. Sawicki and W. Hu, *Phys. Rev. D* **75** (2007), 127502 doi:10.1103/PhysRevD.75.127502 [arXiv:astro-ph/0702278 [astro-ph]].
- [46] V. Faraoni, *Phys. Rev. D* **75** (2007), 067302 doi:10.1103/PhysRevD.75.067302 [arXiv:gr-qc/0703044 [gr-qc]].
- [47] S. Carloni, P. K. S. Dunsby and A. Troisi, *Phys. Rev. D* **77** (2008), 024024 doi:10.1103/PhysRevD.77.024024 [arXiv:0707.0106 [gr-qc]].
- [48] S. Nojiri and S. D. Odintsov, *Phys. Lett. B* **657** (2007), 238-245 doi:10.1016/j.physletb.2007.10.027 [arXiv:0707.1941 [hep-th]].
- [49] N. Deruelle, M. Sasaki and Y. Sendouda, *Prog. Theor. Phys.* **119** (2008), 237-251 doi:10.1143/PTP.119.237 [arXiv:0711.1150 [gr-qc]].
- [50] S. A. Appleby and R. A. Battye, *JCAP* **05** (2008), 019 doi:10.1088/1475-7516/2008/05/019 [arXiv:0803.1081 [astro-ph]].
- [51] E. V. Linder, *Phys. Rev. D* **80** (2009) 123528, arXiv:0905.2962.
- [52] P. K. S. Dunsby, E. Elizalde, R. Goswami, S. Odintsov and D. S. Gomez, *Phys. Rev. D* **82** (2010), 023519 doi:10.1103/PhysRevD.82.023519 [arXiv:1005.2205 [gr-qc]].
- [53] W. Hu and I. Sawicki, *Phys. Rev. D* **76** (2007), 064004 doi:10.1103/PhysRevD.76.064004 [arXiv:0705.1158 [astro-ph]].
- [54] K. Bamba, A. Lopez-Revelles, R. Myrzakulov, S. D. Odintsov and L. Sebastiani, *Class. Quant. Grav.* **30** (2013), 015008 doi:10.1088/0264-9381/30/1/015008 [arXiv:1207.1009 [gr-qc]].
- [55] S. D. Odintsov, V. K. Oikonomou, I. Giannakoudi, F. P. Fronimos and E. C. Lymperiadou, *Symmetry* **15** (2023) no.9, 1701, [arXiv:2307.16308 [gr-qc]].
- [56] S. D'Onofrio, S. Odintsov and T. Schiavone, [arXiv:2511.06924 [gr-qc]].
- [57] S. D. Odintsov, D. Saez-Chillon Gomez, G. S. Sharov. *Eur. Phys. J. C* **77** (2017) 862, arXiv:1709.06800.
- [58] S. D. Odintsov, D. Saez-Chillon Gomez and G. S. Sharov, *Phys. Rev. D.* **99** (2019) 024003, arXiv:1807.02163.
- [59] S. D. Odintsov, D. Sáez-Chillón Gómez and G. S. Sharov, *Phys. Dark Univ.* **42** (2023) 101369, [arXiv:2310.20302 [gr-qc]].
- [60] L. Modesto and L. Rachwal, *Int. J. Mod. Phys. D* **26** (2017) no.11, 1730020; E. Belgacem, Y. Dirian, S. Foffa and M. Maggiore, *JCAP* **1803** (2018) 002 doi:10.1088/1475-7516/2018/03/002 [arXiv:1712.07066 [hep-th]]; A. S. Koshelev, L. Modesto, L. Rachwal and A. A. Starobinsky, *JHEP* **1611** (2016) 067 doi:10.1007/JHEP11(2016)067 [arXiv:1604.03127 [hep-th]].
- [61] S. Deser and R. P. Woodard, *Phys. Rev. Lett.* **99** (2007), 111301 doi:10.1103/PhysRevLett.99.111301 [arXiv:0706.2151 [astro-ph]].
- [62] C. Deffayet and R. P. Woodard, *JCAP* **08** (2009), 023 doi:10.1088/1475-7516/2009/08/023 [arXiv:0904.0961 [gr-qc]].
- [63] S. Deser and R. P. Woodard, *JCAP* **11** (2013), 036 doi:10.1088/1475-7516/2013/11/036 [arXiv:1307.6639 [astro-ph.CO]].
- [64] S. Deser and R. P. Woodard, *JCAP* **06** (2019), 034 doi:10.1088/1475-7516/2019/06/034 [arXiv:1902.08075 [gr-qc]].
- [65] S. Nojiri and S. D. Odintsov, *Phys. Lett. B* **659** (2008) 821 doi:10.1016/j.physletb.2007.12.001 [arXiv:0708.0924 [hep-th]].
- [66] S. Nojiri, S. D. Odintsov, M. Sasaki and Y. I. Zhang, *Phys. Lett. B* **696** (2011) 278 doi:10.1016/j.physletb.2010.12.035 [arXiv:1010.5375 [gr-qc]].
- [67] L. Joukovskaya, *Phys. Rev. D* **76** (2007) 105007 doi:10.1103/PhysRevD.76.105007 [arXiv:0707.1545 [hep-th]].
- [68] G. Calcagni, M. Montobbio and G. Nardelli, *Phys. Lett. B* **662** (2008) 285 doi:10.1016/j.physletb.2008.03.024 [arXiv:0712.2237 [hep-th]].
- [69] S. Jhingan, S. Nojiri, S. D. Odintsov, M. Sami, I. Thongkool and S. Zerbini, *Phys. Lett. B* **663** (2008) 424

- doi:10.1016/j.physletb.2008.04.054 [arXiv:0803.2613 [hep-th]]
- [70] S. Capozziello, E. Elizalde, S. Nojiri and S. D. Odintsov, *Phys. Lett. B* **671** (2009) 193 doi:10.1016/j.physletb.2008.11.060 [arXiv:0809.1535 [hep-th]].
- [71] S. Nojiri, S. D. Odintsov and V. K. Oikonomou, *Phys. Dark Univ.* **28** (2020), 100541 doi:10.1016/j.dark.2020.100541 [arXiv:1911.07329 [gr-qc]].
- [72] S. Nojiri, S. Odintsov and V. K. Oikonomou, *Phys. Lett. B* **874** (2026), 140290 doi:10.1016/j.physletb.2026.140290 [arXiv:2601.07879 [gr-qc]].
- [73] E. Calabrese *et al.* [Atacama Cosmology Telescope], *JCAP* **11** (2025), 063 doi:10.1088/1475-7516/2025/11/063 [arXiv:2503.14454 [astro-ph.CO]].
- [74] Y. Akrami *et al.* [Planck], *Astron. Astrophys.* **641** (2020), A10 [arXiv:1807.06211 [astro-ph.CO]].
- [75] P. A. R. Ade *et al.* [BICEP and Keck], *Phys. Rev. Lett.* **127** (2021) no.15, 151301, [arXiv:2110.00483 [astro-ph.CO]].
- [76] S. D. Odintsov and V. K. Oikonomou, *Phys. Lett. B* **797**, 134874 (2019), [arXiv:1908.07555 [gr-qc]]. arXiv:1908.07555
- [77] A. R. Liddle, *Mon. Not. Roy. Astron. Soc.* **377** (2007), L74-L78, [arXiv:astro-ph/0701113 [astro-ph]].
- [78] L. Chen, Q.-G. Huang and K. Wang, *J. Cosmol. Astropart. Phys.* **1902** (2019) 028, arXiv:1808.05724.